Oxygen Vacancy-rich Ultrathin Co_3O_4 Nanosheets as Nano-fillers in Solid-polymer Electrolyte for High Performance Lithium Metal Batteries

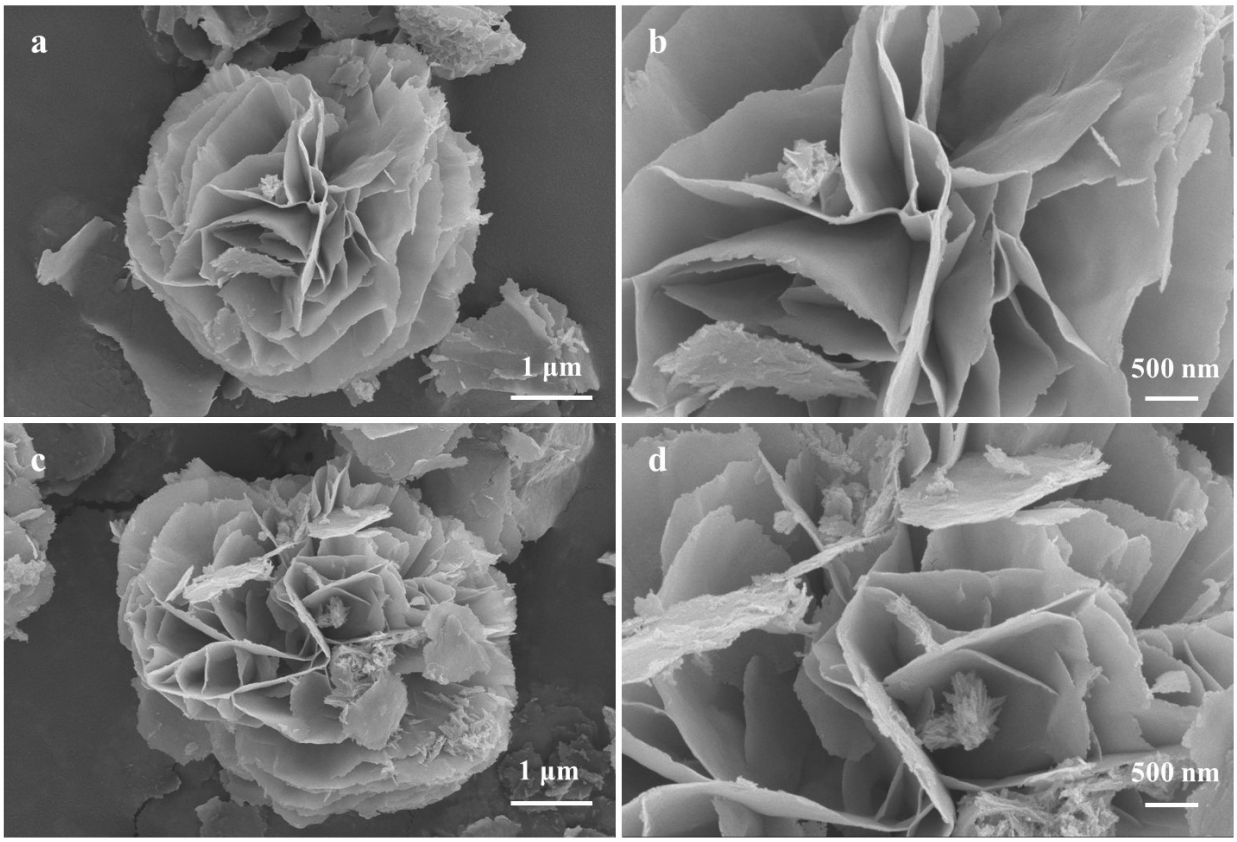

Figure S1. SEM images of (a, b) Co_3O_{4-y}–1 and (c, d) Co_3O_{4-y}–3.

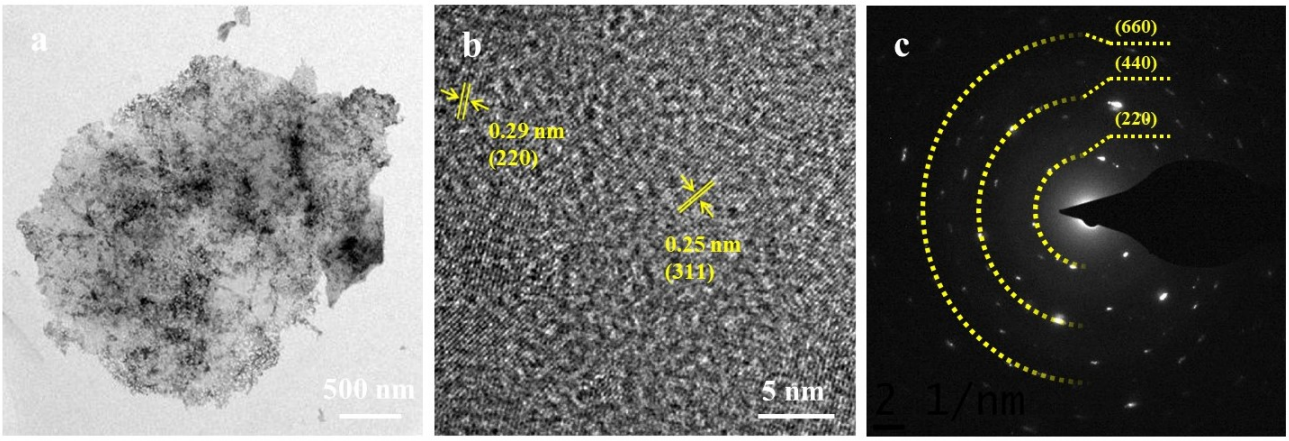

Figure S2. (a, b) TEM images and (c) SEAD patten of Co_3O_4.

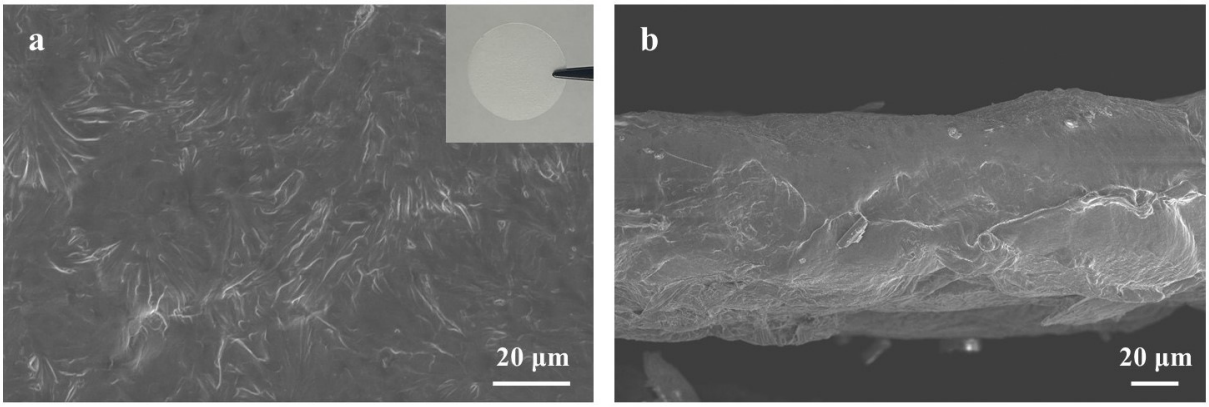

Figure S3. (a) Top-view and (b) side-view SEM images of PEO electrolyte film.

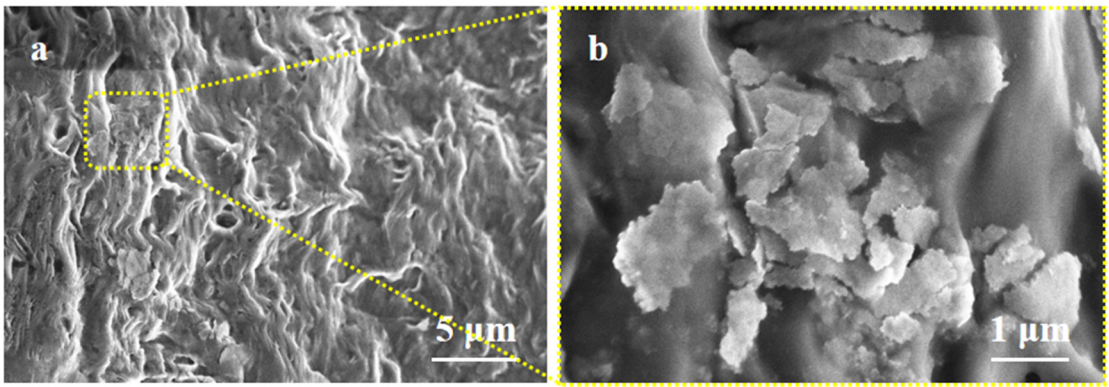

Figure S4. (a) SEM images of PEO/Co_3O_{4-y}–2, (b) enlarged SEM image of rectangular frame.

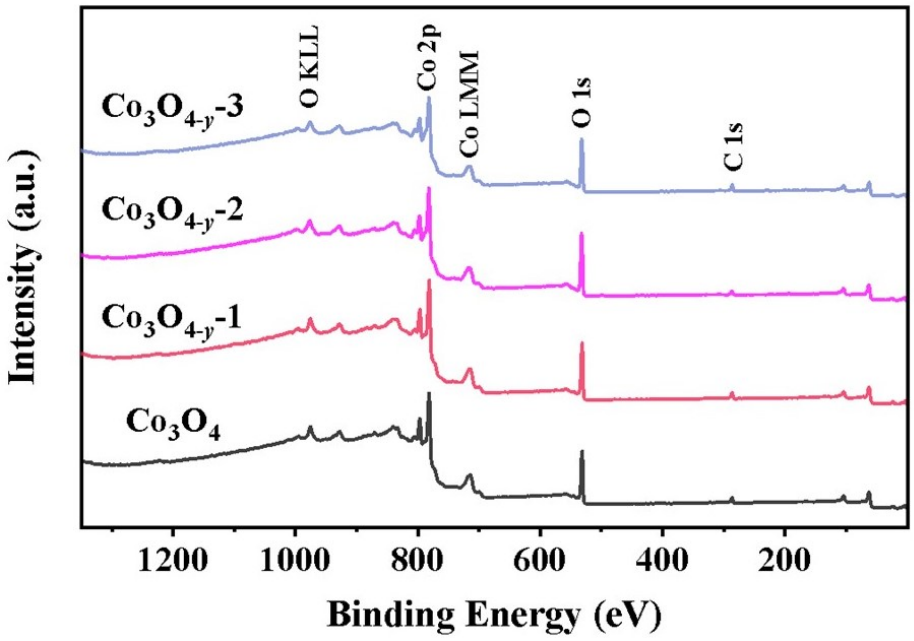

Figure S5. XPS survey spectra of Co_3O_4 and Co_3O_{4-y}–x (x = 1, 2 and 3).

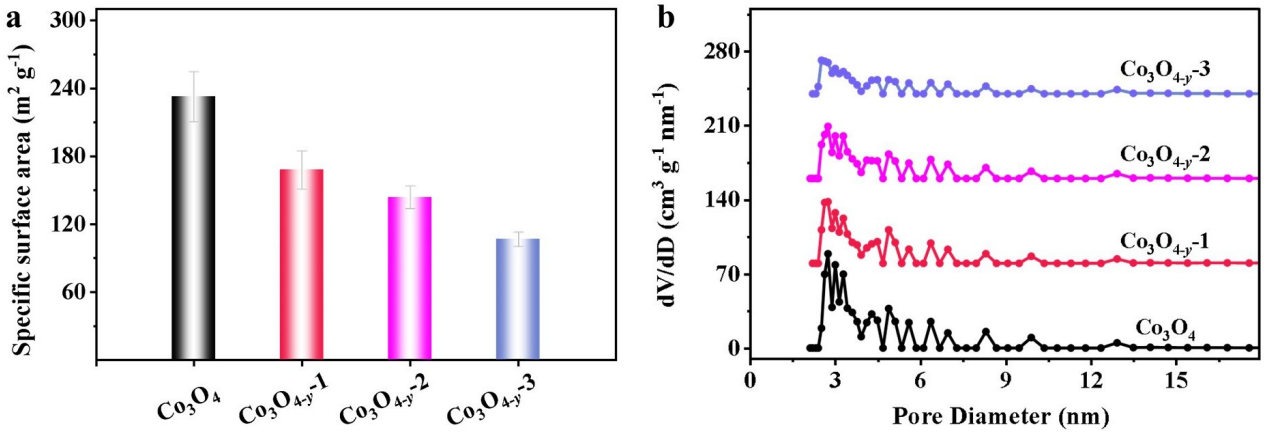

Figure S6. (a) BET specific surface area and (b) pore size distribution of Co_3O_4 and Co_3O_{4-y}–x (x = 1, 2 and 3).

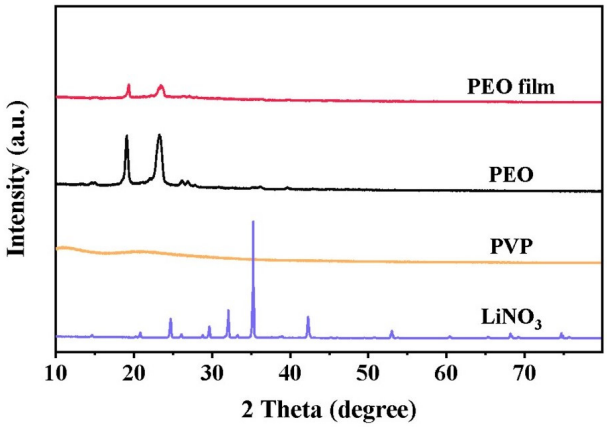

Figure S7. XRD pattens of $LiNO_3$, PVP, PEO and PEO film.

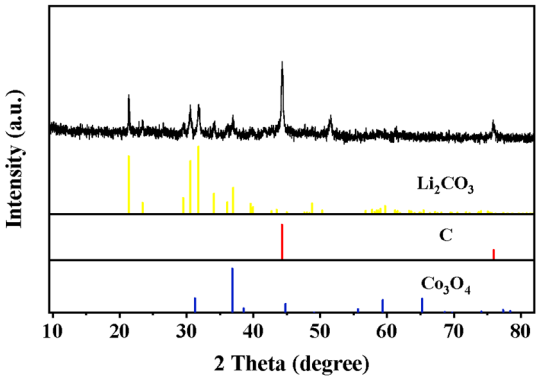

Figure S8. XRD patten of the final residual of PEO/Co_3O_{4-y}–2 after TGA.

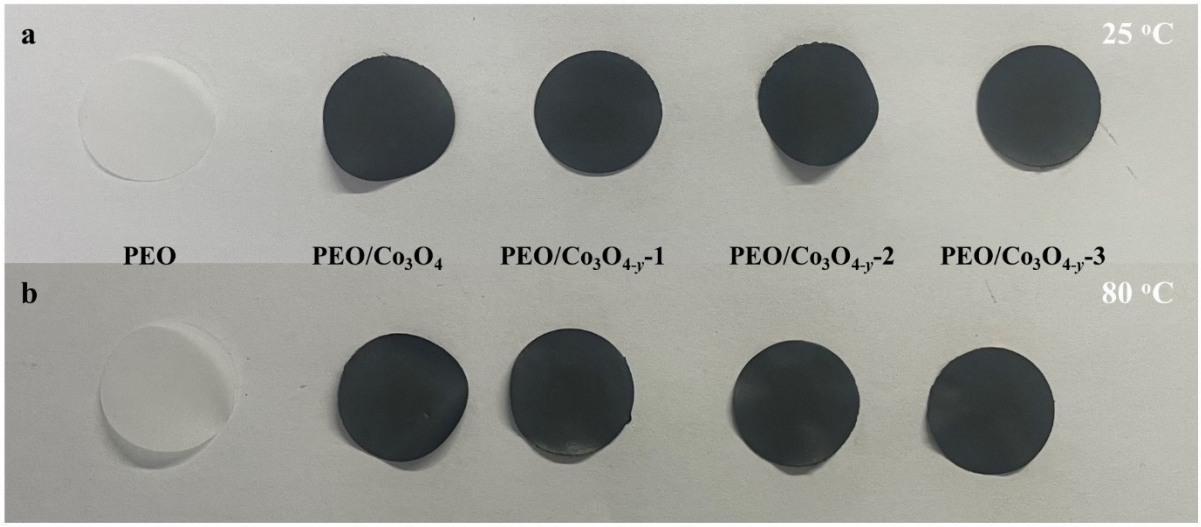

Figure S9. Digital photos of PEO, PEO/Co_3O_4, PEO/Co_3O_{4-y}–1, PEO/Co_3O_{4-y}–2 and PEO/Co_3O_{4-y}–3 films at (a) 25 °C and (b) 80 °C.

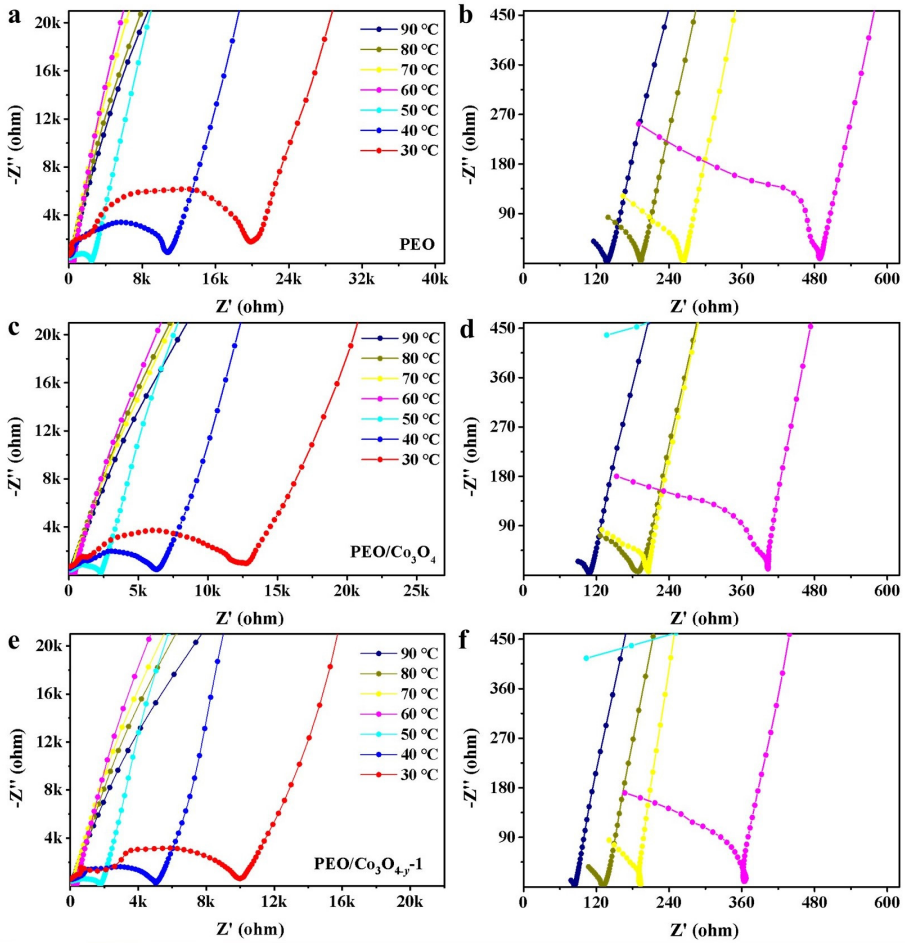

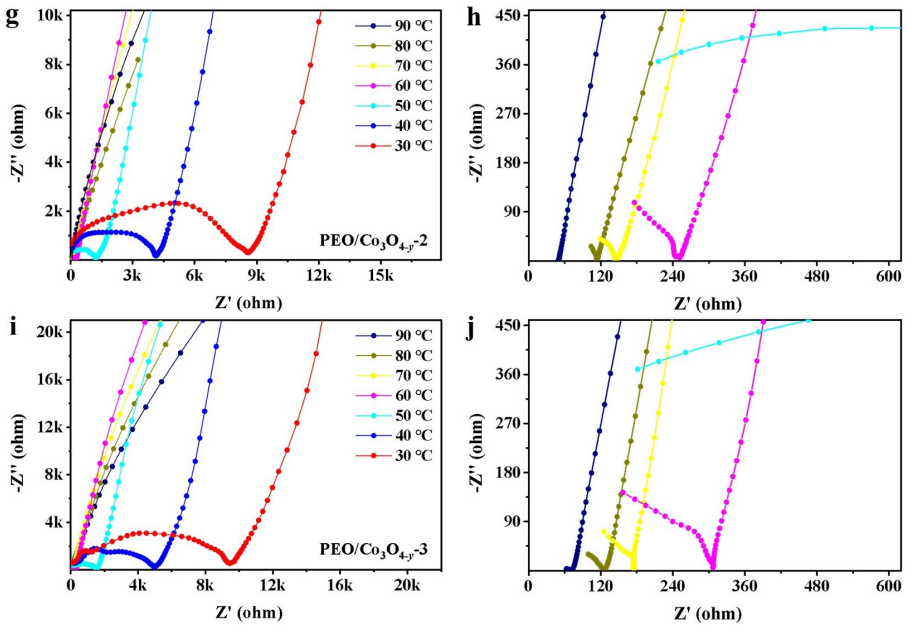

Figure S10. EIS spectra of symmetric SS||SPEs||SS cells using (a, b) PEO, (c, d) PEO/Co_3O_4, (e, f) PEO/Co_3O_{4-y}–1, (g, h) PEO/Co_3O_{4-y}–2 and (i, j) PEO/Co_3O_{4-y}–3 as electrolyte films at 30-90 °C.

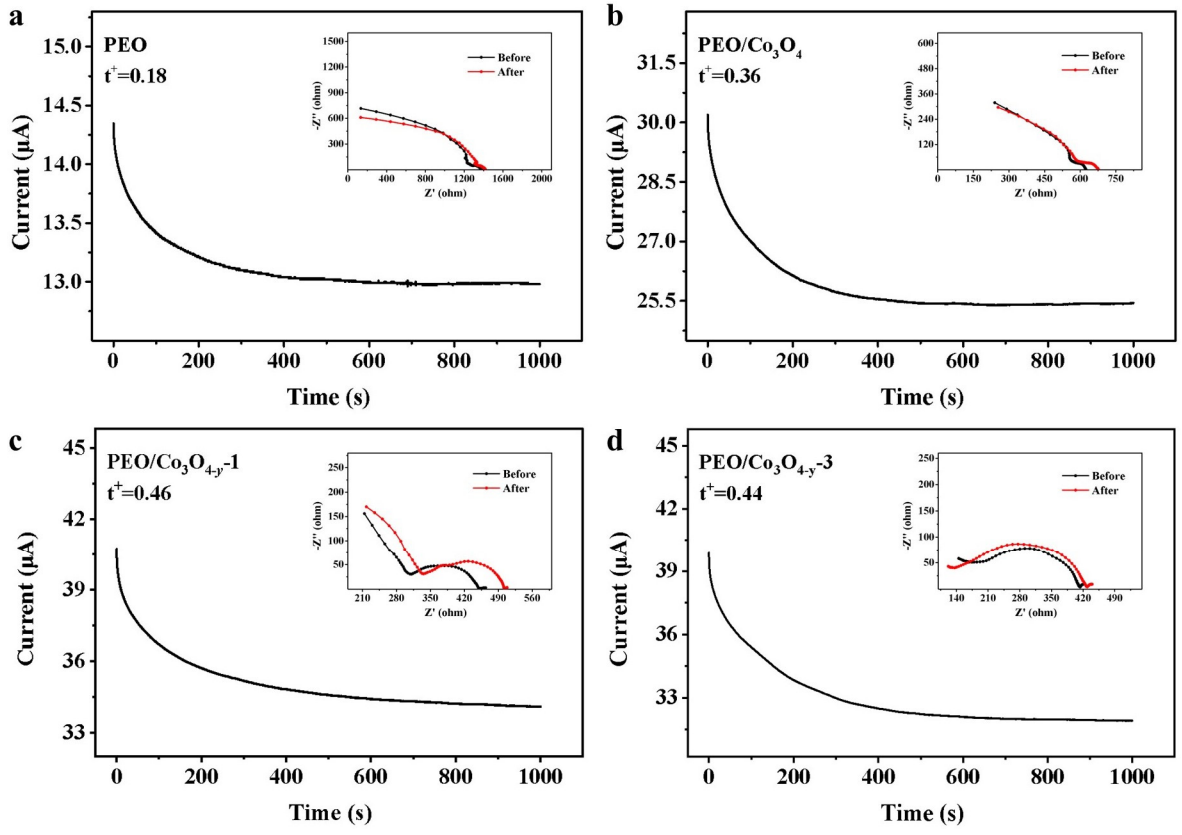

Figure S11. Chronoamperometry curves with a potential step of 20 mV of symmetric Li||SPEs||Li cells using (a) PEO, (b) PEO/Co_3O_4, (c) PEO/Co_3O_{4-y}–1 and (d) PEO/Co_3O_{4-y}–3 as the electrolyte films. Inset: EIS spectra of the cell before and after polarization.

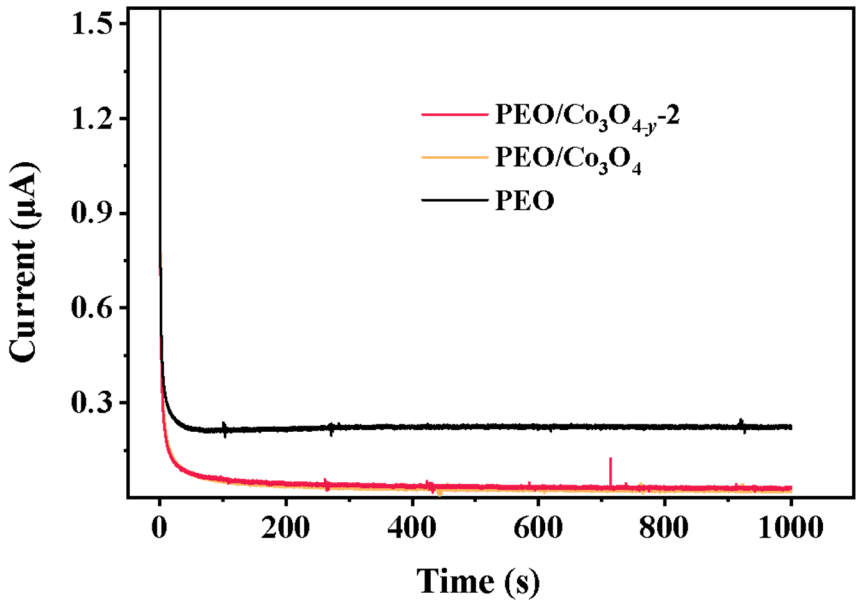

Figure S12. Polarization current–time curve of PEO, PEO/Co_3O_4 and PEO/Co_3O_{4-y}–2 electrolyte with an applied external voltage of 0.1 V.

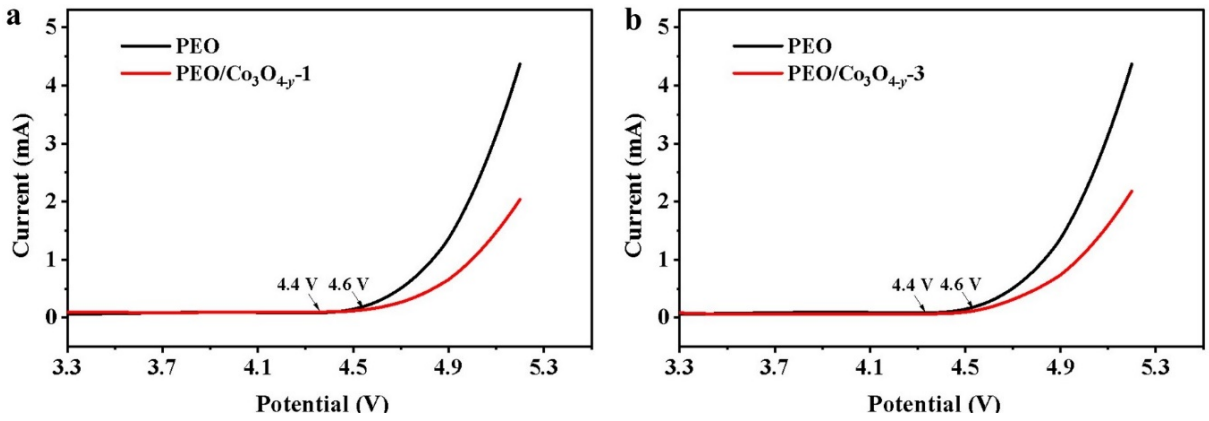

Figure S13. LSV curves at 0.1 mV s^{-1} of asymmetric SS||SPEs||Li cells using (a) PEO/Co_3O_{4-y}–1, (b) PEO/ Co_3O_{4-y}–3 as the electrolyte films.

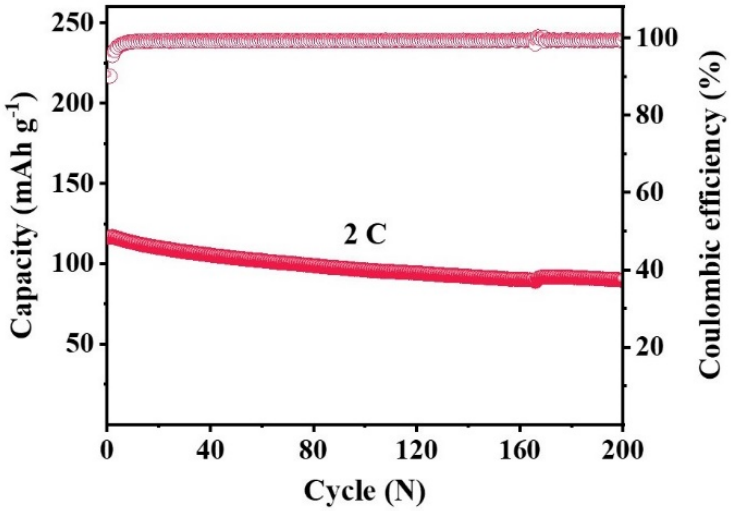

Figure S14. Cycling performance of Li||PEO/Co_3O_{4-y}–2||$LiFePO_4$ cell at 2 C.

Table S1. Detailed XPS and Raman analysis results of Co_3O_4 and Co_3O_{4-y}–x (x = 1, 2 and 3).

Sample	Co^{2+} / Co^{2+}+ Co^{3+} (%)	O_{Ads} / O_{Ads} + O_{Lat} (%)	FWHM
Co_3O_4	37.7	20.9	45.8
Co_3O_{4-y}–1	58.1	33.7	63.4
Co_3O_{4-y}–2	63.4	48.2	82.7
Co_3O_{4-y}–3	68.9	58.9	99.1

Table S2. Pore volume and average pore size of Co_3O_4 and Co_3O_{4-y}–x (x = 1, 2 and 3).

Sample	Pore volume (cm^3/g)	Average pore size (Å)
Co_3O_4	0.376	41.19
Co_3O_{4-y}–1	0.263	41.59
Co_3O_{4-y}–2	0.238	44.01
Co_3O_{4-y}–3	0.183	42.36

Table S3. R_{ct} data of symmetric SS||SPEs||SS cells using PEO, PEO/Co_3O_4, PEO/Co_3O_{4-y}-x (x = 1, 2 and 3) as the electrolyte films at 30-90 ℃.

Temperature (℃)	Rct (Ω)				
	PEO	PEO/Co_3O_4	PEO/Co_3O_{4-y}–1	PEO/Co_3O_{4-y}–2	PEO/Co_3O_{4-y}–3
90	137	108	84	49	70
80	193	180	131	114	123
70	263	205	191	145	175
60	489	405	361	251	307
50	2475	2291	1772	1211	1527
40	10740	6289	5052	4125	4971
30	19930	12730	10072	8594	9512

Table S4. Comparisons of the electrochemical performance between Co_3O_{4-y} and previous reported nanofillers enhanced SPEs.

Nanofiller	Polymer/lithium salt	Enhancement	Reference
Co_3O_{4-y}		This work	
10 wt.% TiO_2	PEO/$LiClO_4$	$\sigma = 2\times10^{-4}$ S cm^{-1} at 60 °C	[1]
Vermiculite sheets (VS)	PEO/LiTFSI	LFP||CSSE||Li, 167 mA h g^{-1} at 0.1C, 82% capacity retention after 200 cycles at 0.5C	[2]
Y_2O_3-doped ZrO_2	PAN/$LiClO_4$	$\sigma = 1.07\times10^{-5}$ S cm^{-1} at 30 °C	[3]
Ca–CeO_2	PEO/LiTFSI	100 mAh g^{-1} at current density of 2 C, 93 mAh g^{-1} after 200 cycles at 1 C	[4]
SiO_2	PEO/LITFSI/SN	LFP||10I||Li, 148.3 mAh g^{-1} of initial cycle, capacity retention of 88% after 400 cycles at 0.5 C	[5]
LiDGO	PEO/LiTFSI	LFP||CSSE||Li, 157 to 139 mAh g^{-1} after 200 cycles with a low capacity retention of 88.5% at 0.5 C	[6]
3D Ce-MOF	PEO/LiTFSI	Li||CSPE||FeF_3, 604 mAh g^{-1} of initial cycle, 200 mAh g^{-1} after 1200 cycles at 0.5 C	[7]
GO	PEO/LiTFSI	LFP||GO–PEO||Li, 142 mAh g^{-1} of initial cycle, 91% capacity retention after 100 cycles at 0.5 C	[8]
PAN-FMP	PEO/LiTFSI	NMC811||GO–PEO||Li, 141.2 mA h g^{-1} of initial cycle, 124.3 mA h g^{-1} after 160 cycles	[9]
Nano ZnO	PEO/LiTFSI /Pyr_{14}TFSI	$\sigma = 7.1\times10^{-3}$ S cm^{-1} at 80 °C	[10]
MnO_2	PEO/LiTFSI	LFP||CSPE||Li, 110 mAh g^{-1} of initial cycle, 143.5 mAh g^{-1} after 300 cycles at 0.5 C	[11]

References

1. Jung, S.; Kim, D.W.; Lee, S.D.; Cheong, M.; Nguyen, D.Q.; Cho, B.W.; Kim, H.S. Fillers for solid-state polymer electrolytes: Highlight. *Bull. Korean Chem. Soc.* **2009**, *30*, 2355–2361, doi:10.5012/BKCS.2009.30.10.2355.
2. Tang, W.; Tang, S.; Guan, X.; Zhang, X.; Xiang, Q.; Luo, J. High-performance solid polymer electrolytes filled with vertically aligned 2D materials. Adv. Funct. Mater. **2019**, *29*, 1900648, doi:10.1002/adfm.201900648.
3. Liu, W.; Lin, D.; Sun, J.; Zhou, G.; Cui, Y. Improved Lithium Ionic Conductivity in Composite Polymer Electrolytes

with Oxide-Ion Conducting Nanowires. *ACS Nano* **2016**, *10*, 11407–11413, doi:10.1021/acsnano.6b06797.
4. Chen, H.; Adekoya, D.; Hencz, L.; Ma, J.; Chen, S.; Yan, C.; Zhao, H.; Cui, G.; Zhang, S. Stable seamless interfaces and rapid ionic conductivity of Ca–CeO2/LiTFSI/PEO composite electrolyte for high-rate and high-voltage all-solid-state battery. *Adv. Energy Mater.* **2020**, 10, 2000049, doi:10.1002/aenm.202000049.
5. Wang, C.; Yang, T.; Zhang, W.; Huang, H.; Gan, Y.; Xia, Y.; He, X.; Zhang, J. Hydrogen bonding enhanced SiO2/PEO composite electrolytes for solid-state lithium batteries. *J. Mater. Chem. A* **2022**, *10*, 3400–3408, doi:10.1039/D1TA10607D.
6. Yang, Z.; Sun, Z.; Liu, C.; Li, Y.; Zhou, G.; Zuo, S.; Wang, J.; Wu, W. Lithiated nanosheets hybridized solid polymer electrolyte to construct Li+ conduction highways for advanced all-solid-state lithium battery. *J. Power Sources* **2021**, *484*, 229287, doi:10.1016/j.jpowsour.2020.229287.
7. Wu, X.; Chen, K.; Yao, Z.; Hu, J.; Huang, M.; Meng, J.; Ma, S.; Wu, T.; Cui, Y.; Li, C. Metal organic framework reinforced polymer electrolyte with high cation transference number to enable dendrite-free solid state Li metal conversion batteries. *J. Power Sources* **2021**, *501*, 229946, doi:10.1016/j.jpowsour.2021.229946.
8. Wen, J.; Zhao, Q.; Jiang, X.; Ji, G.; Wang, R.; Lu, G.; Long, J.; Hu, N.; Xu, C. Graphene oxide enabledflexible PEO-based solid polymer electrolyte for all-solid-state lithium metal battery. *ACS Appl. Energy Mater.* **2021**, *4*, 3660–3669, doi:10.1021/acsaem.1c00090.
9. Li, C.; Zhou, S.; Dai, L.; Zhou, X.; Zhang, B.; Chen, L.; Zeng, T.; Liu, Y.; Tang, Y.; Jiang, J.; et al. Porous polyamine/PEO composite solid electrolyte for high performance solid-state lithium metal batteries. *J. Mater. Chem. A* **2021**, *9*, 24661–24669, doi:10.1039/D1TA04599G.
10. Nematdoust, S.; Najjar, R.; Bresser, D.; Passerini, S. Understanding the role of nanoparticles in PEO-based hybrid polymer electrolytes for solid-state lithium–polymer batteries. *J. Phys. Chem. C* **2020**, *124*, 27907–27915, doi:10.1021/acs.jpcc.0c08749.
11. Li, Y.; Sun, Z.; Liu, D.; Gao, Y.; Wang, Y.; Bu, H.; Li, M.; Zhang, Y.; Gao, G.; Ding, S. A composite solid polymer electrolyte incorporating MnO2 nanosheets with reinforced mechanical properties and electrochemical stability for lithium metal batteries. *J. Mater. Chem. A* **2020**, *8*, 2021–2032, doi:10.1039/C9TA11542K.